Expedient fabrication of well-defined nanofibres from a macrocycle molecule: solution-controlled self-assembly

L Zang[1]*, M Yen[2], K Balakrishnan[3,4], X Yang[1], and **J S Moore[5]**

[1] Department of Materials Science and Engineering, University of Utah, Salt Lake City, Utah, USA

[2] Materials Technology Center, Southern Illinois University, Carbondale, Illinois, USA

[3] Department of Chemistry and Biochemistry, Southern Illinois University, Carbondale, Illinois, USA

[4] Department of Mechanical Engineering and Materials Science, Rice University, Houston, Texas, USA

[5] Departments of Chemistry and Materials Science and Engineering, University of Illinois at Urbana-Champaign, Urbana, Illinois, USA

The manuscript was received on 03 August 2010 and was accepted after revision for publication on 13 August 2010.

DOI: 10.1243/17403499JNN190

Abstract: In this paper an expedient fabrication of uniform nanofibres from a planar arylene–ethynylene tetracycle molecule is reported. The long-range one-dimensional molecular arrangement, which is mainly due to the favourable π–π stacking between the planar shape-persistent molecules, is conducive to enhancement of the exciton migration along the long axis of nanofibres. Such extended exciton migration allows amplification of the fluorescence quenching of the nanofibre by surface-adsorbed chemical reagents, making it possible to construct sensory films consisting of an entangled mesh of the nanofibres, which possess a high sensing efficacy and fast response in vapour detection of explosives.

Keywords: macrocyclic molecule, nanofibre, self-assembly, emission polarization, fluorescence, sensor, explosive

1 INTRODUCTION

Self-assembly of organic molecules into one-dimensional (1D) nanomaterials (e.g. nanofibres) relies on the control and optimization of intermolecular interactions [**1**]. In general, fabrication of high-quality organic nanofibres with controllable size and morphology is not as advanced as for their inorganic counterparts, which take advantage of the easy control of the ionic crystalline growth of inorganic materials [**2**, **3**]. Consequently, the physical and chemical properties of organic nanofibres have not been as thoroughly understood as those of inorganic nanofibres or nanowires [**4**, **5**].

Although organic nanofibres have been fabricated from various conjugated polymers [**6**–**12**], the crystalline structure of these polymeric materials is often difficult to control owing to the complicated intermolecular interactions and polydispersity of the chain. Recent evidence suggests that π–π interaction can be modulated to facilitate the molecular stacking in the self-assembly of planar aromatic molecules [**1**, **13**–**16**]. This is particularly evident in the larger aromatic molecules such as hexabenzocoronene [**17**, **18**], and perylene tetracarboxylic diimide (PTCDI) [**14**, **19**–**26**]. The large π surface of these molecules provides increased π–π interaction that is dominant over the lateral side-chain association between the molecules, thereby producing a molecular self-assembly primarily along the stacking direction. With careful control of the solution processing, the predominant π–π stacking eventually leads to the formation of nanofibres of high aspect ratios.

Recently, the present authors [**27**] have successfully fabricated ultrafine nanofibres from a planar arylene–ethynylene macrocycle (AEM), specifically an alkoxycarbonyl-substituted carbazole-cornered tetracycle (ACTC). The molecular structure of ACTC

*Corresponding author: Department of Materials Science and Engineering, University of Utah, USTAR Building, 383 Colorow Drive, Salt Lake City, UT 84108, USA.
email: lzang@eng.utah.edu

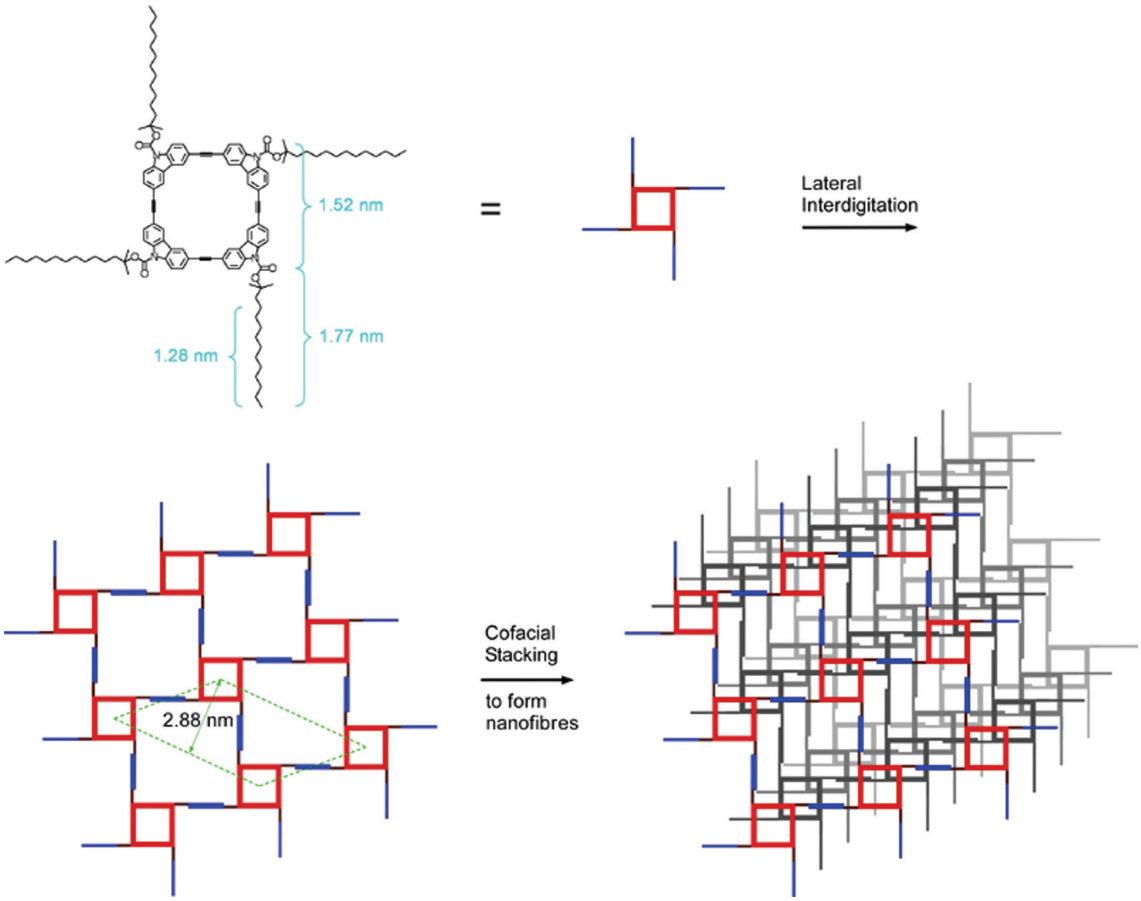

Fig. 1 Energy-minimized configuration of the ACTC molecule obtained by density functional theory calculation (B3LYP/6-31g*) using Gaussian 03, and the proposed one-layer supramolecular assembly through side-chain interdigitation. The primary d spacing for an assembly with 70 per cent side-chain interdigitation is calculated as 2.88 nm, corresponding to a secondary d spacing of 1.44 nm, which is consistent with the value of 1.44 nm measured by X-ray diffraction. The cofacial π–π stacking of the supramolecular planes leads to the formation of nanofibres as depicted by the transmission electron microscopy (TEM) imaging below

is shown in Fig. 1. Because the nanofibres were fabricated through rapid evaporation of solution cast on a substrate, the nanofibres thus obtained were not uniform in terms of size and morphology and were highly entangled together, forming porous thin films. Although these nanofibril films are intrinsically suitable for vapour sensing of the volatile organic compounds, e.g. nitro-aromatic-based explosives (taking advantage of the large surface area and continuous porosity) [**27**, **28**], the fibres suffer from a poorly defined shape, preventing further exploration of the physical and optoelectronic properties and the corresponding applications in nanodevices, particularly at a single-fibre level. Herein, an expedient fabrication of much-better-defined nanofibres from the same ACTC molecule, using solution-based self-assembly processing that is adapted and modified from the methods previously developed for other planar aromatic molecules [**1**], is reported. The new nanofibres thus fabricated can be well dispersed into individual fibres, allowing investigation at a single-fibre level.

2 RESULTS AND DISCUSSION

As previously observed, sol–gel processing is often an effective way to fabricate nanofibril structures from molecules modified with multiple long alkyl side chains [**15**, **29**, **30**]. Gelation of the molecules is typically realized by cooling a hot homogeneous solution from an elevated temperature to room temperature. Such a gelation process decreases gradually the molecular mobility (dynamics) and thus minimizes the lateral growth of the molecular assembly (which is primarily controlled by the side-chain association). Following the sol–gel processing that was previously developed in the present authors' laboratory for a different tetracycle molecule [**29**], gelation of ACTC in cyclohexane was adapted in this study

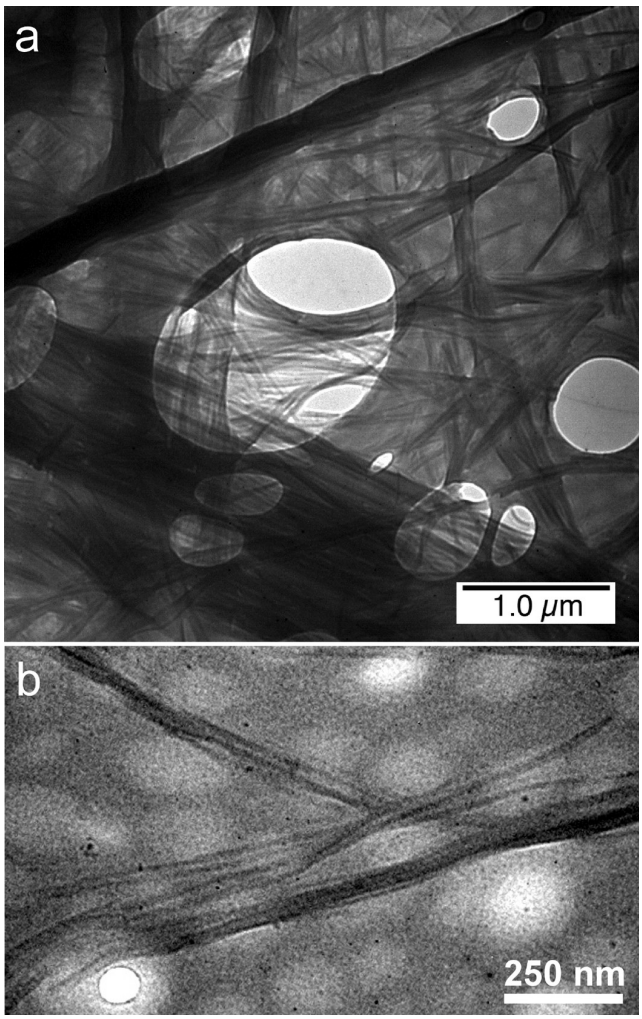

Fig. 2 (a), (b) TEM images of ACTC gel deposited on holey carbon films. The magnified image in (b) shows discrete nanofibres, which were obtained by diluting the as-prepared gel into cyclohexane (about 5 vol% dilution)

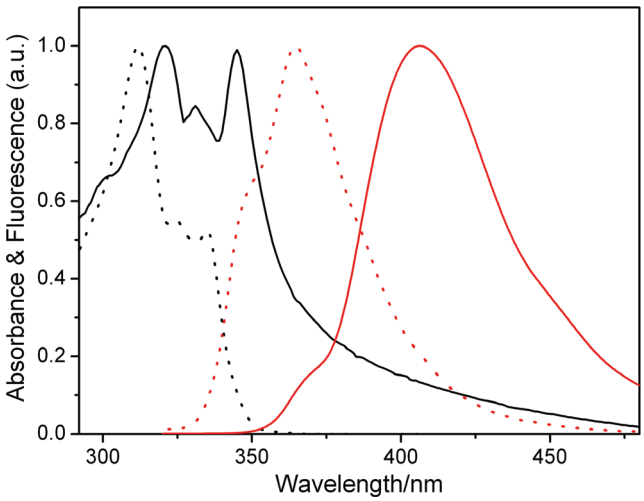

Fig. 3 Absorption (black) and fluorescence (grey) spectra of molecularly dissolved solution (dotted curves) and nanofibres (solid curves) of ACTC (a.u., arbitrary units). The solution concentration was 1 μM in tetrahydrofuran. The nanofibril film was cast from an ACTC gel (three times diluted in cyclohexane). All spectra are normalized to their maxima

to achieve nanofibre self-assembly. The coplanar geometry of ACTC is highly conducive to strong co-facial π–π stacking and thus facilitates the growth of the 1D molecular assembly. Indeed, uniform nanofibres were successfully obtained for ACTC at a low gelation concentration of 1 mg/ml. Figure 2 shows the TEM images of the nanofibres deposited on a holey carbon film, where long fibres with a large aspect ratio are clearly seen all over the substrate; this is the morphological signature that gelation of ACTC is primarily due to the columnar stacking of the macrocycles.

High-magnification imaging indicates discrete nanofibres as presented in Fig. 2(b). The average diameter of the nanofibres is about 10 nm, which corresponds to a cross-section of nine (3 × 3) ACTC molecules laterally associated with maximal interdigitation of side chains (see Fig. 1). The nanofibres thus fabricated are far smaller than most of the nanofibres fabricated from polymers, oligomers, or other planar aromatic molecules, including most discotic molecules [**4**, **6–22**, **31**, **32**]. A small cross-section is usually not thermodynamically favourable for organic nanofibrils with high aspect ratios. The success of fabricating such uniform ultrafine nanofibres from ACTC is possibly due to the strong (multiple) side-chain interdigitation between the molecules, which is facilitated by the coplanar geometry of the molecules. The lateral supramolecular assembly formed by multiple side-chain interdigitation has recently been observed for other AEMs on surfaces by scanning tunnelling microscopy [**33**, **34**].

Consistent with the strong π–π stacking as implicated by the preferred 1D self-assembly, the electronic properties of the ACTC molecule, which is principally determined by the conjugated structure of the core scaffold, is significantly altered when assembled into the fibril structure (Fig. 3). Compared with the absorption spectra of molecules dissolved in solution, the absorption spectrum of the nanofibres deposited on glass is red shifted by 10 nm, and the absorption transition at the lower energy is relatively enhanced. Upon assembly, the fluorescence of individual molecules (centred at 365 nm) is quenched owing to the strong π–π interaction, and instead a new emission band emerges at a longer wavelength, around 405 nm. These spectral changes are characteristic of a π-stacked molecular aggregate [**19**, **32**], for which the collective electronic features

are significantly different from the individual component molecules.

In addition to the sol–gel processing, a 'phase transfer' method (based on slow crystallization at the interface between a 'good' solvent and a 'poor' solvent), which was previously developed in the present authors' laboratory for 1D self-assembly of PTCDI molecules modified with long alkyl side chains [**1**, **20**], was also exploited for the self-assembly of ACTC. The coplanar configuration of ACTC is expected to facilitate the cofacial molecular stacking, and thus the 1D growth of the molecular assembly. Indeed, uniform nanofibres were obtained by phase transfer between a concentrated chloroform solution and an excess of methanol solvent. Figures 4(a) and (b) show the TEM images of the nanofibres grown by this method deposited on silicon oxide and carbon film substrates. The average size of the nanofibres is about 40 nm, about four times larger than those prepared from the sol–gel processing, probably owing to the faster precipitation (crystalline growth) of the molecules in methanol compared with the slow crystallization in gradually cooled cyclohexane.

Interestingly, as shown in Fig. 4, the nanofibres are probably formed through a seeded self-assembly process, for which the initially formed nanocrystals act as the 1D crystalline growing seeds. Similar self-assemblies were previously observed for other organic molecules [**35**, **36**]. Such seeded 1D self-assembly is consistent with the initial fast mixing of the two solvents within the thin layer of interface, where the rapid decrease in the solubility leads to the production of a large number of small nanocrystals, followed by diffusion of more molecules from the chloroform phase to the interface to initiate the 1D growth of nanofibres from the core seeds.

The seeding-induced nanofibril growth can be seen more clearly in the fabrication by rapid dispersion (Fig. 5), where fast injection of a large amount of methanol into a small volume of chloroform solution (1 : 20) created a larger number of nanocrystals. The more seeds thus created, the fewer free molecules are available for the later stage of fibril growth. Indeed, under the same starting concentration of ACTC, the nanofibres fabricated via the rapid dispersion were significantly shorter than those fabricated from the phase transfer processing, as depicted in Fig. 4.

Growing a 1D molecular assembly from fast precipitation requires strong cofacial π–π stacking between the molecules, which dominates the 1D geometry of the molecular assembly. To afford an effective cofacial stacking, a coplanar molecular configuration (including both the core scaffold and the side chains) is usually required to minimize the steric hindrance caused by the out-of-plane side chains. Indeed, when the same phase transfer or rapid dispersion method was applied to tetradecyl tetracycle (TDTC) (a molecule with the same core as ACTC, but in saddle-like geometry with the side chains) [**29**], only ill-defined agglomerates were formed.

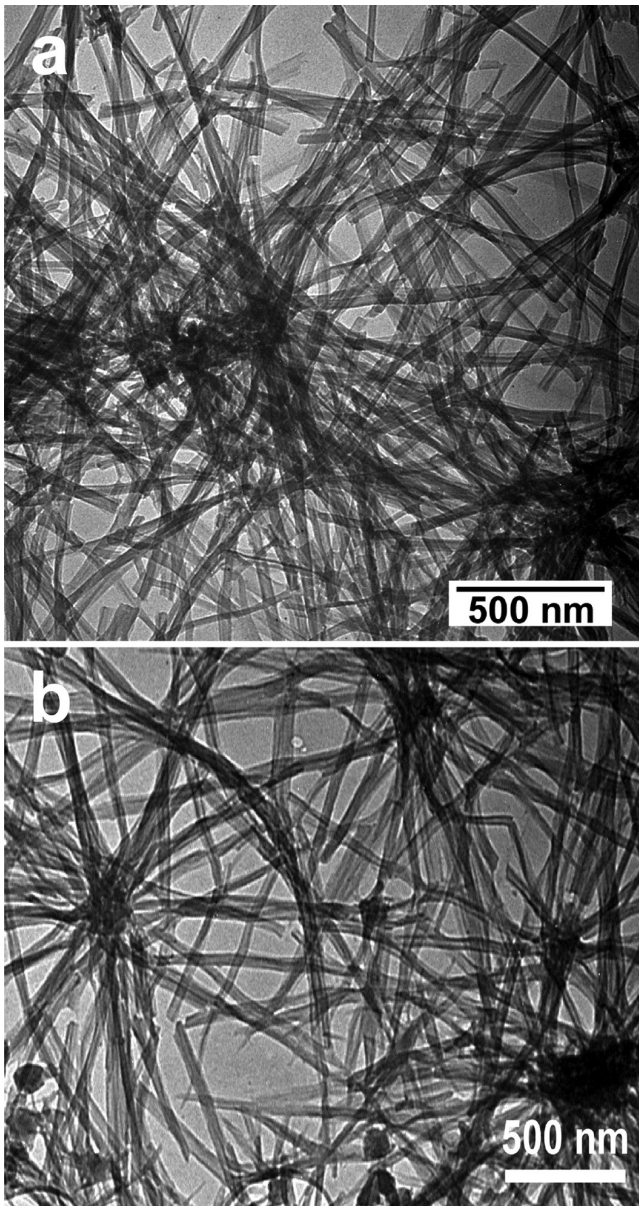

Fig. 4 TEM images of ACTC nanofibres fabricated by phase-transfer crystallization between excessive methanol and a concentrated chloroform solution (1.0 mM). The TEM samples were prepared by depositing the nanofibres on (a) silicon oxide grids and (b) holey carbon films

The strong π–π stacking between the planar ACTC molecules provides the nanofibril structure with sufficient mechanical integrity to be transferred on to different substrates. Compared with the polar substrate of silicon oxide as used in Fig. 4(a), a nonpolar substrate, namely a holey carbon film, was

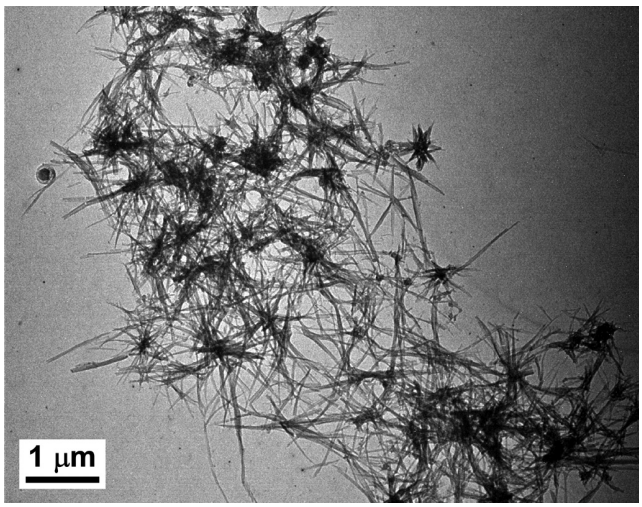

Fig. 5 TEM images of ACTC nanofibres fabricated by rapid dispersion of a concentrated chloroform solution (1.0 mM) into a large volume of methanol (1 : 20 by volume). The TEM sample was prepared by depositing the nanofibres on silicon oxide grids

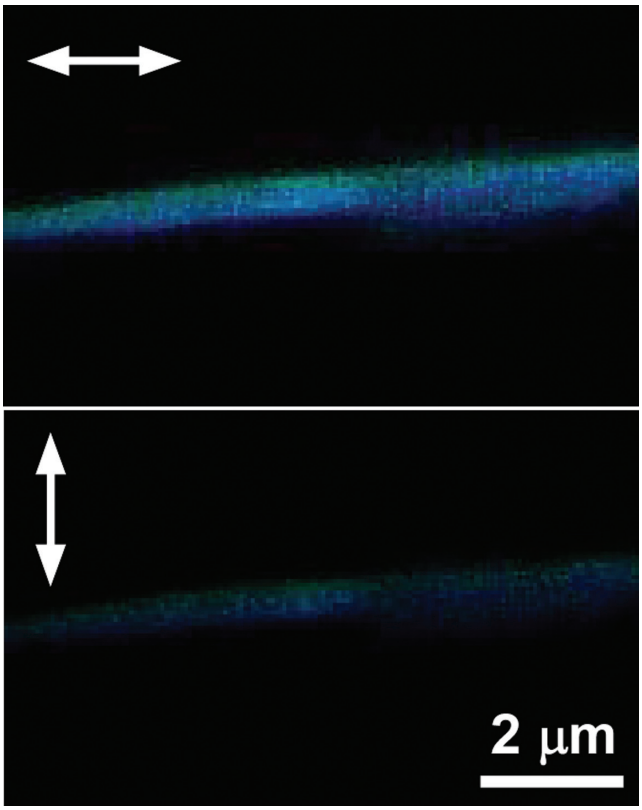

Fig. 6 Fluorescence microscopy images of a single ACTC nanofibre under linearly polarized excitation (340–380 nm). The directions of excitation polarization are labelled with double-headed arrows. Because of the optical diffraction, the fibre in the image appears larger than the size measured by TEM

also employed for TEM imaging of the nanofibres (Fig. 4(b)). The same morphology and fibre distribution were found for the nanofibres deposited on the carbon films. This robust durable character of the nanofibres allows expedient transferral and deposition on to various substrates, which are critical for approaching practical applications of the nanofibres in device fabrication [**32**]. More interestingly, the nanofibres assembled in solutions demonstrated strong stability (against Ostwald ripening) as evidenced by the TEM imaging, for which the nanofibres stored (aged) in the assembling solution for more than 1 month were deposited on to both silicon oxide and carbon films and showed the same size and morphology as those freshly prepared.

Considering the 1D morphology of the nanofibre, which is primarily controlled by the π–π stacking, the nanofibre should demonstrate strong anisotropy in intermolecular electronic coupling, i.e. approximately uniaxial optical properties along the long axis of the nanofibre [**37**]. This is similar to the uniaxial columnar packing of discotic liquid crystal molecules and other planar aromatic molecules [**19**, **22**, **37**, **38**]. Figure 6 shows the fluorescence microscopy image of a single ACTC nanofibre under linearly polarized excitation (340–380 nm). Depending on the orientation of a nanofibre with respect to the excitation polarizer, the fluorescence intensity measured for the nanofibre changes from the minimum when the polarizer is perpendicular to the long axis of the nanofibre, to the maximum when the polarizer is oriented parallel to the nanofibre. Such linearly polarized emission is consistent with the 1D π–π stacking, which typically possesses a transition dipole parallel to the direction of π–π stacking (i.e. perpendicular to the molecular plane), as evidenced in the cofacially stacked dimers of other planar aromatic molecules (e.g. phenalene) [**22**, **24**, **39**].

The 1D molecular stacking between planar aromatic molecules is usually conducive to exciton migration via cofacial intermolecular electronic coupling [**1**, **22**, **40**, **41**]. Consequently, extended exciton diffusion is expected for the ACTC nanofibre along the long axis, which enables amplified fluorescence quenching by surface-adsorbed quenchers to take place, in the same manner as observed for the conjugated polymers [**42**–**44**]. Deposition of a large number of the nanofibres on to a glass substrate formed a highly porous film consisting of an entangled mesh of the nanofibres, as depicted in the TEM images (Figs 2 and 4). Such a nanofibril film not only provides increased surface area to enhance the adsorption of gaseous molecules but also allows expedient diffusion of quencher molecules across the film matrix. Combination of the porous characteristics with the extended exciton migration intrinsic to the individual nanofibre makes

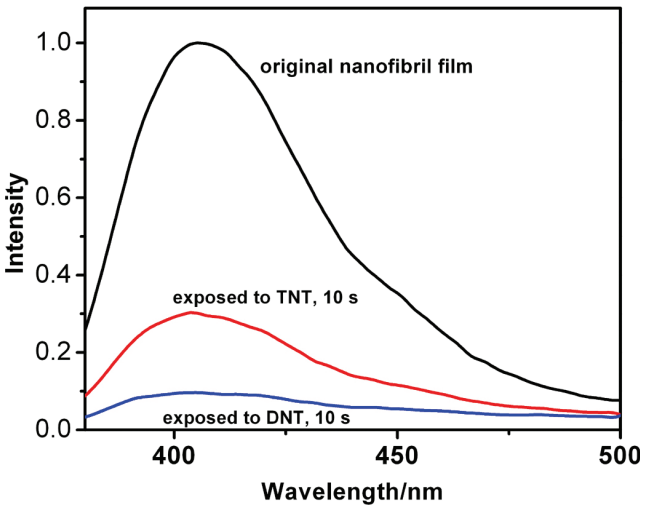

Fig. 7 Fluorescence spectra of a thin layer of ACTC nanofibres (deposited from the gel) upon exposure to the saturated vapour of TNT (5 ppb) and DNT (100 ppb) for 10 s. Before use in the quenching, the deposited film was dried in a vacuum oven at 60 °C for 3 h. The average thickness of the film was 75 nm

the nanofibril film an efficient sensing material for detecting oxidative volatile organic compounds (VOCs), particularly the nitro-aromatic explosives, which act as electron acceptors to quench the fluorescence of the ACTC nanofibres. Moreover, the ultrafine size of the nanofibres fabricated in this study provides increased surface area for the sensory film. An increased surface area will potentially enhance the surface adsorption, and thus the sensing efficiency, when used in the detection of VOCs. Indeed, the nanofibres as described demonstrated efficient fluorescence quenching upon exposure to the vapour of nitro-aromatic explosives such as 2,4,6-trinitrotoluene (TNT) and 2,4-dinitrotoluene (DNT) (Fig. 7), and both the quenching efficiency and the response time were significantly improved in comparison with those of the poor-quality nanofibres fabricated from the direct surface vaporization method [**27**]. This is probably due to the enlarged porosity and surface area thus formed by the better-defined nanofibres, as illustrated by the TEM imaging in Figs 2 and 4.

3 CONCLUSIONS

An expedient fabrication of uniform nanofibres from a planar AEM molecule is reported in this paper. Drop casting of the nanofibres on to a substrate produces a highly porous film consisting of an entangled mesh of nanofibres. This film fabrication technique enables 'bottom-up' optimization of the materials property through molecular design and engineering. This is in contrast with the conventional fabrication of polymer films, for which the properties and functions are strongly dependent on the post-casting treatment. Moreover, the recently developed expedient chemical synthesis of AEMs and related structures [**45–47**] allows modification of the core scaffold with reducing moieties to increase the electron-donating capability of the whole molecule. An increased reducing power is conducive to enhancing the fluorescence quenching, and thus the sensing for oxidative VOCs, which act as the electron acceptors. The expedient fabrication of nanofibres as reported in this study, together with the high adaptability of AEM synthesis, provides wide options for developing various nanofibre-based sensing materials for detecting oxidative VOCs, particularly the nitro-aromatic explosives.

4 EXPERIMENTAL DETAILS

4.1 Materials and general methods

DNT (97 per cent) was purchased from Fisher, and TNT (99 per cent) was purchased from Chemservice. All other molecules and solvents (high-performance liquid chromatography or spectroscopic grade) were purchased from Fisher or Aldrich and used as received. ACTC was synthesized following the protocol as described in reference [**27**]. All air- or moisture-sensitive manipulations were performed under argon protection using standard Schlenk techniques or in an argon-filled glove box.

Ultraviolet (UV)-visible absorption and fluorescence spectra were measured on a PerkinElmer Lambda 25 spectrophotometer and LS 55 fluorometer (equipped with a solid sample holder) respectively. TEM measurement was performed with a Hitachi 7100 (operated at 100 kV). The sample was prepared by drop casting the diluted gel of ACTC or the nanofibril suspension in methanol on to a TEM grid (coated with either holey carbon or silicon oxide film), followed by drying in air overnight. Fluorescence microscopy imaging was carried out with a Leitz Orthoplan II microscope equipped with a real-colour charge-coupled device camera for recording the emission image. A Hoechst Stain Filter set was used to allow UV excitation (340–380 nm) and collection of the emission above 430 nm. A linear polarizer plate was used to modulate the excitation polarization.

4.2 Fabrication of ACTC nanofibres

4.2.1 Method 1: gelation

Ultrafine nanofibres of ACTC were fabricated through a gelation process in cyclohexane, a method that was successfully used for fabricating ultrafine

nanofibres from TDTC [**29**]. Briefly, 1 mg of the solid ACTC was added to 1 ml of cyclohexane in a tube; a milky suspension was thus obtained by sonicating the suspension for 5 min. Upon heating in an oil bath at 100 °C, the milky suspension became totally dissolved, producing a transparent solution. During cooling slowly to room temperature, the solution turned turbid within a few minutes because of the initiation of the molecular aggregation, which eventually led to gelation. Leaving the sample under ambient conditions without disturbing it for 1 h led to the formation of an aged gel, as revealed by the phase immobilization. The gel formation for ACTC occurred only in cyclohexane, while other solvents such as toluene, tetrahydrofuran, dioxane, hexane, and chloroform did not result in gelation.

4.2.2 Method 2: phase transfer

Uniform nanofibres of ACTC were also fabricated through a so-called phase transfer method, which has been developed in the present authors' laboratory for assembling large planar aromatic molecules into 1D nanostructures (e.g. nanowires) [**22**]. Briefly, the molecular assembly was processed through slow crystallization at the interface between a good solvent and a poor solvent, where the slow phase transfer between the two solvents decreases the solubility at the interface. The poor solvent (e.g. methanol) is normally quite different (e.g. in terms of polarity) from the good solvent (e.g. chloroform), thus providing the possibility of keeping the two solvents in separate phases for an extended period. Typically, a larger amount (greater than 10 : 1 by volume) of poor solvent was transferred atop a concentrated chloroform solution of the molecule (1 mM) in a test tube. Within minutes, crystallization (precipitation) occurred at the interface of the two solvents (seen as a band), followed by slow diffusion into the upper phase of the poor solvent. The crystals thus formed can be transferred and cast on to different substrates.

4.2.3 Method 3: rapid dispersion

Nanofibril self-assembly of ACTC was also performed through fast precipitation by rapidly dispersing the molecules from a good solvent (such as chloroform) into a poor solvent (such as methanol), where the molecule has limited solubility and thus self-assembly of the molecules is expected to occur instantaneously. Briefly, a minimum volume of a concentrated chloroform solution (1 mM) of ACTC was injected rapidly into a larger volume (1 : 20 by volume) of methanol, followed by immediate mixing with a pipette. Such a self-assembly approach has the advantage of the strong intermolecular π–π interaction, which is enhanced in a poor solvent owing to the solvophobic interaction.

4.3 Fluorescence-quenching measurement

The fluorescence quenching by DNT and TNT was monitored following a similar method to that previously developed by Yang and Swager [**48**]. Briefly, the fluorescence spectra of the nanofibril film were measured immediately after immersing inside a sealed jar (50 ml) containing a small amount of the explosives (TNT or DNT). To prevent direct contact of the film with the explosive analytes, some cotton was used to cover the explosive powder deposited at the bottom of the jar. Before use the jar was sealed overnight to achieve a constant saturated vapour pressure inside. The presence of cotton also helps to maintain a constant vapour pressure.

ACKNOWLEDGEMENTS

This work was supported by the National Science Foundation (Grants CAREER CHE 0641353 and CBET 730667), the US Department of Homeland Security (Cooperative Agreement 2009-ST-108-LR0005), and the USTAR Program.

REFERENCES

1 **Zang, L., Che, Y.,** and **Moore, J. S.** One-dimensional self-assembly of planar π-conjugated molecules: adaptable building blocks for organic nanodevices. *Accts Chem. Res.*, 2008, **41**, 1596–1608.

2 **Hu, J., Odom, T. W.,** and **Lieber, C. M.** Chemistry and physics in one dimension: synthesis and properties of nanowires and nanotubes. *Accts Chem. Res.*, 1999, **32**, 435–445.

3 **Xia, Y., Yang, P., Sun, Y., Wu, Y., Mayers, B., Gates, B., Yin, Y., Kim, F.,** and **Yan, H.** One-dimensional nanostructures: synthesis, characterization, and applications. *Advd Mater.*, 2003, **15**, 353–389.

4 **Schenning, A. P. H. J.** and **Meijer, E. W.** Supramolecular electronics; nanowires from self-assembled p-conjugated systems. *Chem. Commun.*, 2005, 3245–3258.

5 **Grimsdale, C. A.** and **Müllen, K.** The chemistry of organic nanomaterials. *Angew. Chem., Int. Edn*, 2005, **44**, 5592–5629.

6 **Huang, J. X., Virji, S., Weiller, B. H.,** and **Kaner, R. B.** Polyaniline nanofibers: facile synthesis and chemical sensors. *J. Am. Chem. Soc.*, 2003, **125**, 314–315.

7 **Zhou, Y., Freitag, M., Hone, J., Staii, C.,** and **Johnson, J. A. T.** Fabrication and electrical characterization of polyaniline-based nanofibers with diameter below 30 nm. *Appl. Phys. Lett.*, 2003, **83**, 3800–3802.

8 **Liu, H., Kameoka, J., Czaplewski, D. A.,** and **Craighead, H. G.** Polymeric nanowire chemical sensor. *Nano Lett.*, 2004, **4**, 671–675.

9 **Lee, H. J., Jin, Z. X., Aleshin, A. N., Lee, J. Y., Goh, M. J., Akagi, K., Kim, Y. S., Kim, D. W.,** and **Park, Y. W.** Dispersion and current-voltage characteristics of helical polyacetylene single fibers. *J. Am. Chem. Soc.*, 2004, **126**, 16 722–16 723.

10 **Zhang, X.** and **Manohar, S. K.** Narrow pore-diameter polypyrrole nanotubes. *J. Am. Chem. Soc.*, 2005, **127**, 14 156–14 157.

11 **Bocharova, V., Kiriy, A., Vinzelberg, H., Mönch, I.,** and **Stamm, M.** Polypyrrole nanowires grown from single adsorbed polyelectrolyte molecules. *Angew. Chem. Int. Edn*, 2005, **44**, 6391–6394.

12 **Luo, Y. H., Liu, H. W., Xi, F., Li, L., Jin, X. G., Han, C. C.,** and **Chan, C. M.** Supramolecular assembly of poly(phenylene vinylene) with crown ether substituents to form nanoribbons. *J. Am. Chem. Soc.*, 2003, **125**, 6447–6451.

13 **Nguyen, T.-Q., Martel, R., Avouris, P., Bushey, M. L., Brus, L.,** and **Nuckolls, C.** Molecular interactions in one-dimensional organic nanostructures. *J. Am. Chem. Soc.*, 2004, **126**, 5234–5242.

14 **Wurthner, F.** Perylene bisimide dyes as versatile building blocks for functional supramolecular architectures. *Chem. Commun.*, 2004, 1564–1579.

15 **Shirakawa, M., Fujita, N.,** and **Shinkai, S.** A stable single piece of unimolecularly π-stacked porphyrin aggregate in a thixotropic low molecular weight gel: a one-dimensional molecular template for polydiacetylene wiring up to several tens of micrometers in length. *J. Am. Chem. Soc.*, 2005, **127**, 4164–4165.

16 **Wang, Z., Medforth, C. J.,** and **Shelnutt, J. A.** Porphyrin nanotubes by ionic self-assembly. *J. Am. Chem. Soc.*, 2004, **126**, 15 954–15 955.

17 **Hill, J. P., Jin, W., Kosaka, A., Fukushima, T., Ichihara, H., Shimomura, T., Ito, K., Hashizume, T., Ishii, N.,** and **Aida, T.** Self-assembled hexa-*peri*-hexabenzocoronene graphitic nanotube. *Science*, 2004, **304**, 1481–1483.

18 **Wu, J., Pisula, W.,** and **Müllen, K.** Graphenes as potential material for electronics. *Chem. Rev.*, 2007, **107**, 718–747.

19 **Balakrishnan, K., Datar, A., Oitker, R., Chen, H., Zuo, J.,** and **Zang, L.** Nanobelt self-assembly from an organic n-type semiconductor: propoxyethyl-PTCDI. *J. Am. Chem. Soc.*, 2005, **127**, 10 496–10 497.

20 **Balakrishnan, K., Datar, A., Naddo, T., Huang, J., Oitker, R., Yen, M., Zhao, J.,** and **Zang, L.** Effect of side-chain substituents on self-assembly of perylene diimide molecules: morphology control. *J. Am. Chem. Soc.*, 2006, **128**, 7390–7398.

21 **Datar, A., Oitker, R.,** and **Zang, L.** Surface-assisted one-dimensional self-assembly of a perylene based semiconductor molecule. *Chem. Commun.*, 2006, 1649–1651.

22 **Datar, A., Balakrishnan, K., Yang, X. M., Zuo, X., Huang, J. L., Yen, M., Zhao, J., Tiede, D. M.,** and **Zang, L.** Linearly polarized emission of an organic semiconductor nanobelt. *J. Phys. Chem.*, 2006, **110**, 12 327–12 332.

23 **Che, Y., Yang, X., Liu, G., Yu, C., Ji, H., Zuo, J., Zhao, J.,** and **Zang, L.** Ultrathin n-type organic nanoribbons with high photoconductivity and application in optoelectronic vapor sensing of explosives. *J. Am. Chem. Soc.*, 2010, **132**, 5743–5750.

24 **Che, Y., Yang, X., Balakrishnan, K., Zuo, J.,** and **Zang, L.** Highly polarized and self-waveguided emission from single-crystalline organic nanobelts. *Chem. Mater.*, 2009, **21**, 2930–2934.

25 **Che, Y., Datar, A., Balakrishnan, K.,** and **Zang, L.** Ultralong nanobelts self-assembled from an asymmetric perylene tetracarboxylic diimide. *J. Am. Chem. Soc.*, 2007, **129**, 7234–7235.

26 **Che, Y., Datar, A.,Yang, X., Naddo, T., Zhao, J.,** and **Zang, L.** Enhancing one-dimensional charge transport through intermolecular π-electron delocalization: conductivity improvement for organic nanobelts. *J. Am. Chem. Soc.*, 2007, **129**, 6354–6355.

27 **Naddo, T., Che, Y., Zhang, W., Balakrishnan, K., Yang, X., Yen, M., Zhao, J., Moore, J. S.,** and **Zang, L.** Detection of explosives with a fluorescent nanofibril film. *J. Am. Chem. Soc.*, 2007, **129**, 6978–6979.

28 **Naddo, T., Yang, X., Moore, J. S.,** and **Zang, L.** Highly responsive fluorescent sensing of explosives taggant with an organic nanofibril film. *Sensors Actuators: B. Chem.*, 2008, **134**, 287–291.

29 **Balakrishnan, K., Datar, A., Zhang, W., Yang, X., Naddo, T., Huang, J., Zuo, J., Yen, M., Moore, J. S.,** and **Zang, L.** Nanofibril self-assembly of an arylene ethynylene macrocycle. *J. Am. Chem. Soc.*, 2006, **128**, 6576–6577.

30 **Shirakawa, M., Fujita, N.,** and **Shinkai, S.** [60]fullerene-motivated organogel formation in a porphyrin derivative bearing programmed hydrogen-bonding sites. *J. Am. Chem. Soc.*, 2003, **125**, 9902–9903.

31 **Grimsdale, A. C.** and **Müllen, K.** The chemistry of organic nanomaterials. *Angew. Chem. Int. Edn*, 2005, **44**, 5592–5629.

32 **Hoeben, F. J. M., Jonkheijm, P., W. Meijer, E.,** and **Schenning, A. P. H. J.** About supramolecular assemblies of π-conjugated systems. *Chem. Rev.*, 2005, **105**, 1491–1546.

33 **Grave, C.** and **Schluter, A. D.** Shape-persistent nanosized macrocycles. *Eur. J. Org. Chem.*, 2002, 3075–3098.

34 **Pan, G.-B., Cheng, X.-H., Hoeger, S.,** and **Freyland, W.** 2D supramolecular structures of a shape-persistent macrocycle and co-deposition with fullerene on HOPG. *J. Am. Chem. Soc.*, 2006, **128**, 4218–4219.

35 **Genson, K. L., Holzmueller, J., Ornatska, M., Yoo, Y.-S., Par, M.-H., Lee, M.,** and **Tsukruk, V. V.** Assembling of dense fluorescent supramolecular webs via self-propelled star-shaped aggregates. *Nano Lett.*, 2006, **6**, 435–440.

36 **Yan, P., Chowdhury, A., Holman, M. W.,** and **Adams, D. M**. Self-organized perylene diimide nanofibers. *J. Phys. Chem. B*, 2005, **109**, 724–730.

37 **Friedrich, M., Wagner, T., Salvan, G., Park, S., Kampen, T. U.,** and **Zahn, D. R. T.** Optical constants of 3,4,9,10-perylenetetracarboxylic dianhydride films on silicon and gallium arsenide studied by spectroscopic ellipsometry. *Appl. Phys. A*, 2002, **75**, 501–506.

38 Pisula, W., Tomoviæ, Z., Stepputat, M., Kolb, U., Pakula, T., and **Müllen, K.** Uniaxial alignment of polycyclic aromatic hydrocarbons by solution processing. *Chem. Mater.*, 2005, **17**, 2641–2647.

39 Small, D., Zaitsev, V., Jung, Y., Rosokha, S. V., Head-Gordon, M., and **Kochi, J. K.** Intermolecular π-to-π bonding between stacked aromatic dyads. experimental and theoretical binding energies and near-IR optical transitions for phenalenyl radical/radical versus radical/cation dimerizations. *J. Am. Chem. Soc.*, 2004, **126**, 13 850–13 858.

40 Hughes, R. E., Hart, S. P., Smith, D. A., Movaghar, B., Bushby, R. J., and **Boden, N.** Exciton dynamics in a one-dimensional self-assembling lyotropic discotic liquid crystal. *J. Phys. Chem. B*, 2002, **106**, 6638–6645.

41 Hoffmann, M., Schmidt, K., Fritz, T., Hasche, T., Agranovich, V. M., and **Leo, K.** The lowest energy Frenkel and charge-transfer excitons in quasi-one-dimensional structures: application to MePTCDI and PTCDA crystals. *Chem. Phys.*, 2000, **258**, 73–96.

42 McQuade, D. T., Pullen, A. E., and **Swager, T. M.** Conjugated polymer-based chemical sensors. *Chem. Rev.*, 2000, **100**, 2537–2574.

43 Yang, J.-S. and **Swager, T. M.** Porous shape persistent fluorescent polymer films: an approach to TNT sensory materials. *J. Am. Chem. Soc.*, 1998, **120**, 5321–5322.

44 Zhou, Q. and **Swager, T. M.** Fluorescent chemosensors based on energy migration in conjugated polymers: the molecular wire approach to increased sensitivity. *J. Am. Chem. Soc.*, 1995, **117**, 12 593–12 602.

45 Zhao, D. and **Moore, J. S.** Shape-persistent arylene ethynylene macrocycles: syntheses and supramolecular chemistry. *Chem. Commun.*, 2003, 807–818.

46 Zhang, W. and **Moore, J. S.** Shape-persistent macrocycles: structures and synthetic approaches from arylene and ethynylene building blocks. *Angew. Chem., Int. Edn*, 2006, **45**, 4416–4439.

47 Hartley, C. S., Elliott, E. L., and **Moore, J. S.** Covalent assembly of molecular ladders. *J. Am. Chem. Soc.*, 2007, **129**, 4512–4513.

48 Yang, J.-S. and **Swager, T. M.** Fluorescent porous polymer films as TNT chemosensors: electronic and structural effects. *J. Am. Chem. Soc.*, 1998, **120**, 11 864–11 873.